

AgenticDiffusion: Agentic Diffusion-based Path Planning for Vision-Based UAV Navigation

Faryal Batool Muhammad Ahsan Mustafa Fawad Mehboob Valerii Serpiva

Dzmitry Tsetserukou

Abstract: Indoor UAV navigation requires efficient exploration, scene understanding, and reliable trajectory execution under limited field-of-view observations. Existing vision-based navigation frameworks typically rely on single-view observations, limiting their ability to reason about occlusions, target visibility, and global scene structure. In this work, we propose **AgenticDiffusion**, a multi-view UAV navigation framework that coordinates language-guided reasoning, open-vocabulary target grounding, vision-based diffusion planning, and NMPC within a unified aerial navigation pipeline. Given a natural language instruction and synchronized first-person-view (FPV) and top-view observations, the framework determines the most informative viewpoint for navigation and generates a mission plan prior to trajectory execution. The targets are localized using an open-vocabulary grounding model, after which viewpoint-specific diffusion planners generate navigation trajectories for UAV execution. Using complementary viewpoints, the proposed framework reduces repeated target exploration and improves navigation efficiency in cluttered indoor environments. The framework was validated in four real-world UAV navigation scenarios involving adaptive viewpoint selection, multi-stage mission execution, long-horizon navigation, and safe landing-site selection. The experimental results demonstrated an overall mission success rate of 80% in 40 real-world trials, while the diffusion planners achieved a trajectory generation success rate of 100%.

Keywords: UAV Navigation, Multi-View Navigation, Diffusion Planning, Semantic Navigation, Vision-Language Navigation

1 Introduction

Autonomous UAV navigation in indoor environments requires robots to reason about semantic task objectives while taking into account obstacle layouts and scene accessibility. Most existing navigation systems rely on single visual observations, limiting their ability to reason about occlusions, target visibility, and global scene structure. As a result, such systems often require repeated semantic inference for effective environment exploration and understanding. Recent advances in learning-based navigation, including reinforcement learning [1], diffusion-based planners [2, 3], and vision-language navigation frameworks [4], have demonstrated promising performance for autonomous navigation. However, these methods typically operate from a single viewpoint and do not reason over complementary visual perspectives to determine which viewpoint is most informative for a given semantic navigation objective.

To address these limitations, we propose **AgenticDiffusion**, an agentic multi-view navigation framework for an autonomous UAV that combines semantic reasoning, target-view association, mission planning, diffusion based trajectory planning, and NMPC based trajectory execution for semantic aerial navigation in indoor environments. Given a natural language instruction and synchronized top-view and first-person-view (FPV) observations, the proposed framework localizes semantic targets using Grounding DINO [5] and reasons over both views to determine which targets are visible and which planning modality is most suitable for navigation in each of them. The framework also

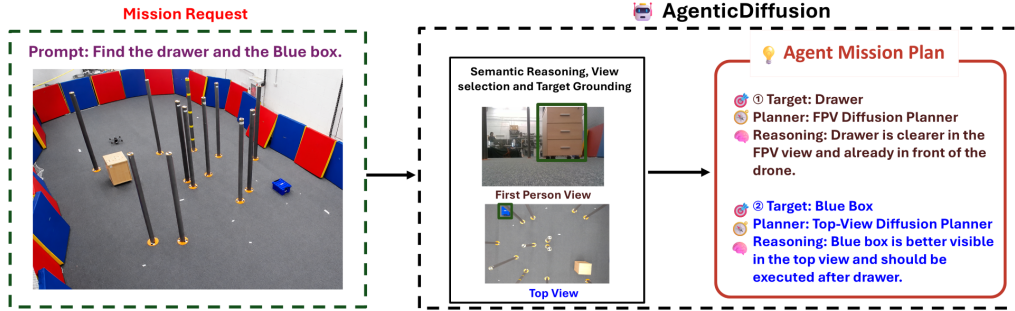


Figure 1: Multi-view semantic reasoning and adaptive mission planning in AgenticDiffusion for a scenario.

performs mission-level reasoning prior to trajectory execution, enabling sequential target scheduling, planner-aware navigation, and reducing repeated semantic inference during exploration. Using complementary visual perspectives, the proposed framework improves semantic exploration efficiency and reduces ambiguity caused by limited field-of-view observations as illustrated in Fig. 1. The main contributions of this paper are:

- We propose **AgenticDiffusion**, a unified multi-view UAV navigation framework integrating language-guided reasoning, open-vocabulary grounding, diffusion-based trajectory planning, and NMPC-based execution.
- We introduce a mission-level multi-view reasoning pipeline that associates semantic targets with the most informative viewpoint and generates an executable navigation plan prior to trajectory execution.
- We validate the proposed framework in four real-world indoor UAV navigation scenarios involving sequential target navigation, adaptive planner selection, and semantic landing-site reasoning, while demonstrating direct simulation-to-real deployment of the diffusion planners without additional fine-tuning.

2 Related Works

Autonomous UAV navigation in indoor environments remains challenging due to occlusions, limited field-of-view observations, dynamic obstacles, and ambiguity in semantic target localization. Recent advances in learning-based planning, embodied reasoning, and vision-language navigation have significantly improved autonomous decision-making and trajectory generation. However, most existing approaches rely on fixed observation modalities and do not reason jointly across complementary viewpoints for mission-level navigation tasks.

2.1 Learning-Based and Diffusion Navigation Frameworks

Learning-based navigation methods have demonstrated strong capabilities for obstacle-aware navigation and long-horizon trajectory generation [1, 6, 7]. More recently, diffusion-based planners such as NoMaD [3], NavDP [2], and related trajectory generation frameworks [8, 9, 10, 11] have shown promising performance for visual navigation and mapless planning. These methods generate feasible trajectories directly from visual observations and improve navigation robustness in cluttered environments. However, existing approaches primarily operate from a single viewpoint and do not incorporate viewpoint-aware reasoning or mission-level planner selection for aerial navigation.

2.2 Multi-View and Spatial Navigation Frameworks

Multi-view perception and navigation methods have been explored to improve environmental awareness and robustness under viewpoint-limited observations. Prior works investigated multi-view reinforcement learning [12], multi-camera UAV perception and SLAM systems [13, 14], and coor-

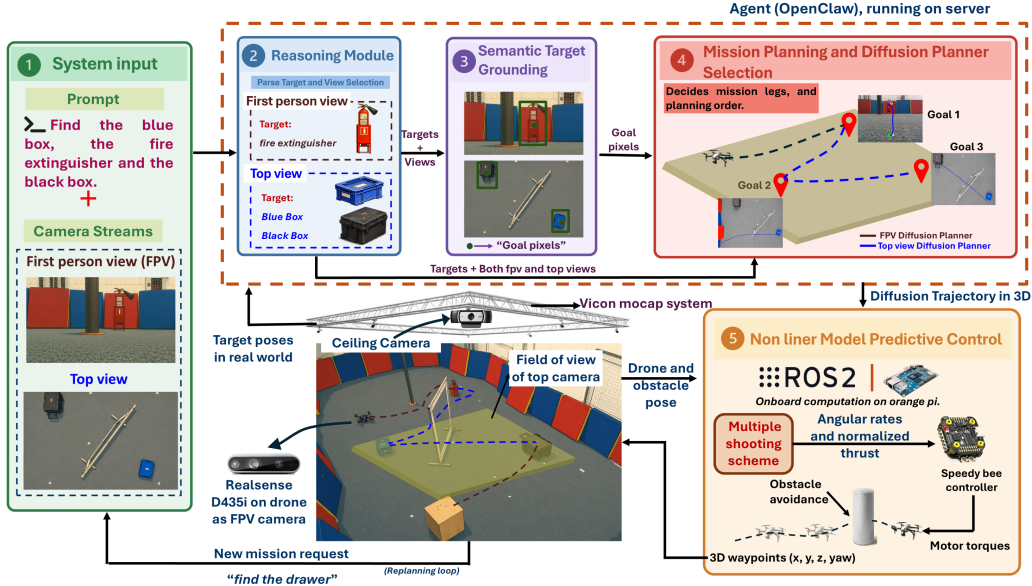


Figure 2: Overview of the proposed AgenticDiffusion framework. Given a natural language instruction and synchronized FPV and top-view observations, the agent performs semantic target interpretation, multi-view reasoning, open-vocabulary grounding, mission planning, and diffusion planner selection. The generated trajectories are executed on the UAV using an NMPC in a receding-horizon control loop.

dedicated viewpoint-aware navigation pipelines [15, 16]. In parallel, spatial reasoning and language-grounded mapping frameworks such as VLMs [17], SpatialVLM [18], and MapNav [19] improved scene understanding for embodied agents. Memory-guided exploration and synthetic VLN training approaches [20, 21] further enhanced semantic exploration capabilities. Nevertheless, these methods do not jointly integrate synchronized multi-view reasoning, target grounding, and vision-based UAV trajectory planning within a unified navigation framework.

2.3 Agentic Vision-Language Navigation Frameworks

Recent embodied AI systems increasingly leverage VLMs, LLMs, and agentic reasoning for instruction-guided navigation and mission planning. Vision-language navigation frameworks such as NaVid [4], Fast-SmartWay [22], JanusVLN [23], and related embodied navigation agents [24, 25] demonstrated strong capabilities for language-conditioned navigation and target understanding. More recent agentic systems including Voyager [26], SMART-LLM [27], hierarchical UAV agents [28], and FlowAgent [29] highlighted the growing role of hierarchical reasoning and generative planning in embodied robotics.

In contrast to existing approaches, the proposed AgenticDiffusion framework integrates mission-level multi-view reasoning, open-vocabulary grounding, diffusion-based trajectory generation, and predictive UAV control within a unified aerial navigation pipeline. By jointly reasoning across synchronized FPV and top-view observations, the proposed framework enables viewpoint-aware semantic navigation and planner selection prior to trajectory execution.

3 Methodology

The proposed **AgenticDiffusion** framework shown in Fig. 2, operates as a hierarchical multi-view UAV navigation pipeline. Given a user instruction together with synchronized FPV and top-view observations, the framework first determines which targets are visible and which viewpoint is most suitable for navigation. The selected targets are then localized, organized into an executable mission plan, converted into view-specific diffusion trajectories, and finally executed using an onboard

NMPC controller. OpenClaw is used as the agentic reasoning framework, while Claude Sonnet 4.6 is used for instruction understanding, viewpoint selection, and mission planning [30, 31].

3.1 Semantic Target Parsing and View Selection

The framework first interprets the user instruction and extracts an ordered list of navigation targets from synchronized FPV and top-view observations. The two camera views are spatially separated to provide complementary environmental coverage for multi-view reasoning. Given a command such as “*find the drawer and the blue box*”, the reasoning module identifies the requested targets for downstream navigation. After target extraction, the framework analyzes both observation streams to determine which viewpoint is most suitable for each target. The reasoning module evaluates target visibility and navigation suitability across the FPV and top-view images before assigning a planner to each navigation task. For example, the blue box may be clearly visible in the top-view image while partially occluded in the FPV observation. Even when a target appears in both views, the framework selects the observation that provides better spatial and visual context for navigation.

3.2 Open-Vocabulary Target Grounding

After viewpoint selection, the framework localizes each target within the selected observation using Grounding DINO [5]. Given an image-target pair, the grounding module predicts the target bounding box and corresponding image-space coordinates. The center point of the predicted bounding box is used as the goal pixel and forwarded to the mission planning module. Only detections with confidence scores above 0.3 are considered valid for navigation. The grounding stage additionally supports candidate-aware reasoning for tasks involving multiple detections, such as selecting the least cluttered landing site or identifying the nearest medical bag relative to a detected human target.

3.3 Agentic Mission Planning

After target grounding, the framework generates an executable mission plan by jointly reasoning over the drone position, selected viewpoints, grounded targets, and environmental layout. During mission initialization, the planning module determines the execution order of navigation tasks and assigns the appropriate planner to each target. For targets selected from the top-view observation, the grounded image coordinates are projected into world coordinates and associated with the nearest VICON-tracked object. In practice, the projected target locations were typically within 0.2–0.4 m of the corresponding VICON-tracked objects. Once associated, the VICON-tracked target is used for mission-state monitoring and target-completion verification during execution. For FPV navigation, target locations are obtained directly in the world frame through depth-assisted projection and therefore do not require additional matching.

Using the resulting target positions, the agent generates an ordered sequence of navigation legs together with the corresponding planner assignments and goal locations. The world-frame target information is also used as a feedback signal to determine whether the UAV has reached the current target and should transition to the next stage of the mission. The generated mission plan therefore specifies the target identity, navigation goal, selected planner, and execution order for each navigation task. If a requested object is not detected, the framework can optionally prompt the user to retry the search using a modified prompt or detection threshold.

3.4 Vision-Based Diffusion Trajectory Planning

The proposed framework utilizes image-conditioned diffusion planners for both FPV and top-view navigation. Once the target coordinates are obtained from the grounding module, the corresponding planner generates a trajectory conditioned on the start point, RGB observation, and target goal. The top-view planner generates long-horizon trajectories using global scene observations, enabling efficient navigation across cluttered indoor environments. In contrast, the FPV planner produces short-horizon egocentric trajectories for nearby targets using first-person observations. Both planners are

trained entirely in simulation and directly deployed in real-world experiments without additional fine-tuning. Detailed implementation and mathematical formulations of the diffusion planners are provided in the Appendix.

3.5 NMPC-Based Trajectory Execution

The NMPC module serves as the control layer that executes the trajectory generated by the diffusion planner while ensuring dynamically feasible UAV motion and obstacle avoidance. The generated trajectory is converted into a receding-horizon reference for the NMPC. The controller uses a continuous-time quaternion based quadrotor model to predict the UAV motion, with CasADi [32] used for symbolic model and cost construction and acados [33] used to solve the resulting constrained optimal control problem. This allows the UAV to accurately track the planned path while maintaining a stable attitude, regulating the velocity and angular rates, and avoiding obstacles. The mathematical formulation of the NMPC is described in the Appendix.

4 Experimental Setup and Results

The proposed AgenticDiffusion framework was evaluated in real-world indoor UAV navigation experiments involving multi-target navigation, adaptive viewpoint selection, and mission-level planning. The high-level reasoning and diffusion planning modules were executed on a desktop PC equipped with an NVIDIA RTX 5090 GPU and 24 GB RAM, while trajectory execution was performed onboard a custom-built quadrotor equipped with a SpeedyBee flight controller, an Orange Pi 5B onboard computer, and an Intel RealSense D435i camera operating at 15 Hz. A Logitech C930ce camera was used to provide top-view observations. The FPV and top-view cameras were spatially separated by more than 1.8 m to provide complementary environmental coverage and reduce overlap between the two observation streams. Communication between the planning and control modules was established through a ROS2-based distributed architecture, while the NMPC controller operated at 100 Hz.

For FPV navigation, grounded image coordinates were projected into 3D world coordinates using aligned depth observations from the RealSense camera. For top-view navigation, pixel-to-world transformation was performed using geometric projection based on the known camera height. The framework was evaluated across four indoor navigation scenarios designed to validate viewpoint-aware target selection, sequential mission execution, long-horizon navigation, and semantic landing-site reasoning. Each scenario was repeated 10 times to evaluate system robustness under real-world operating conditions.

4.1 Scenario 1: Multi-Stage Multi-View Semantic Navigation

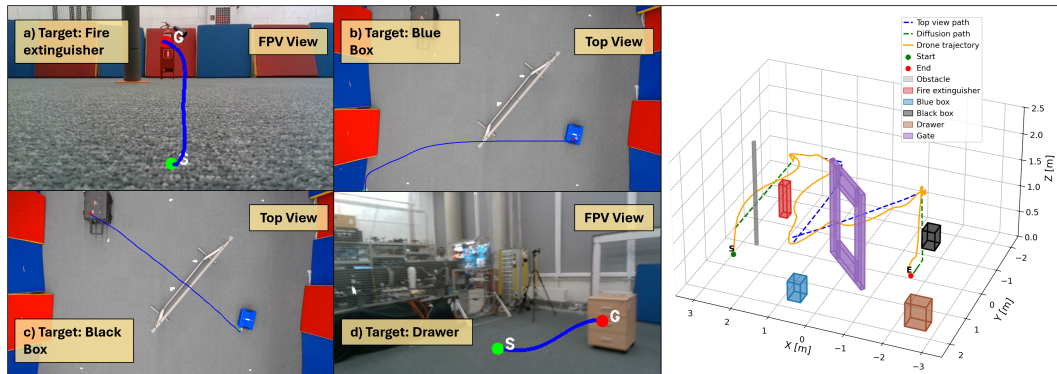


Figure 3: Scenario 1: Sequential multi-view navigation toward the fire extinguisher, blue box, black box, and drawer using FPV and top-view diffusion planning.

The first experiment evaluated the proposed framework in a sequential multi-target navigation task, as shown in Fig. 3. The user prompt was: “find the blue box, fire extinguisher, and the black box.” During mission initialization, the agent determined that the fire extinguisher was best suited for FPV navigation, while the blue box and black box were more suitable for top-view planning. The generated mission plan therefore first executed FPV navigation toward the fire extinguisher, followed by top-view navigation toward the blue box and the black box.

A new user request was then issued to find the drawer. Since the drawer was primarily visible in the FPV stream, the framework generated an FPV-based trajectory toward the final target. This experiment demonstrates the capability of the proposed framework to perform multi-stage semantic navigation using mission-level multi-view reasoning and planner-aware trajectory execution. The framework achieved a success rate of 80% (8/10 trials), while the remaining failures were caused by communication loss between the VICON system and the UAV.

4.2 Scenario 2: Adaptive Multi-View Target Selection

The second experiment evaluated the ability of the framework to select the most suitable viewpoint when a target was visible in multiple observations, as shown in Fig. 4. The user prompt was: “find the drawer and the blue box.” During mission initialization, the agent determined that the drawer was more clearly visible in the FPV image, while the blue box was only reliably visible in the top-view observation. The generated mission plan therefore first executed FPV navigation toward the drawer, followed by top-view navigation toward the blue box. This experiment demonstrates the capability of the proposed framework to perform viewpoint-aware target association and planner selection prior to trajectory execution. The framework for this scenario achieved a success rate of 70% (7/10 trials). The remaining failures occurred in highly cluttered environments where the NMPC obstacle-avoidance cost caused the UAV to converge to locally optimal hovering behavior near obstacles, instead of producing a sufficiently large deviation to bypass the obstruction and rejoin the reference path. Although larger avoidance maneuvers could reduce this behavior, aggressive trajectory deviations were constrained by the limited VICON tracking region, where leaving the capture area could result in localization loss during flight.

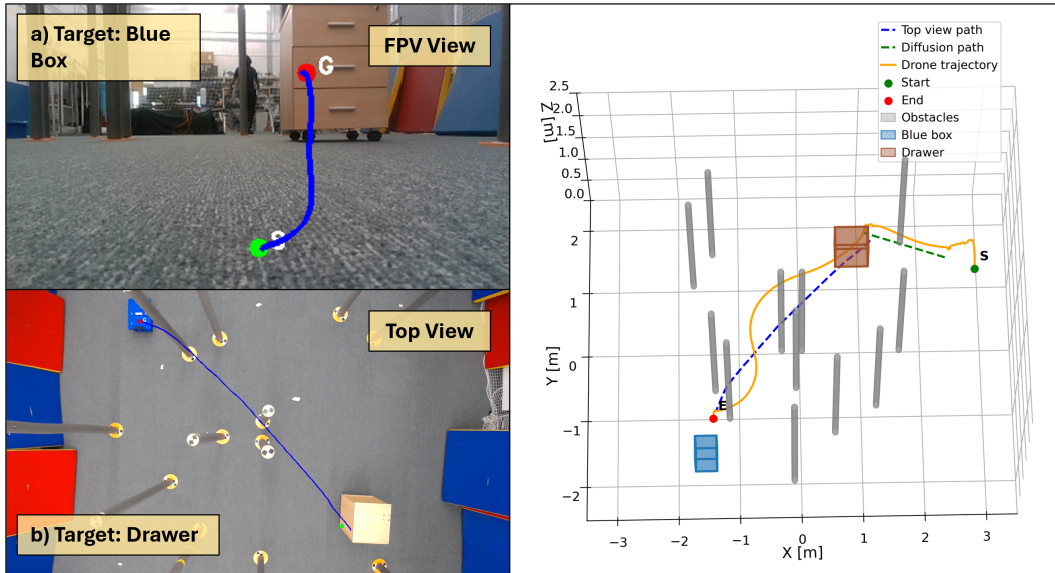


Figure 4: Scenario 2: Adaptive multi-view target selection for sequential FPV and top-view navigation toward the drawer and blue box.

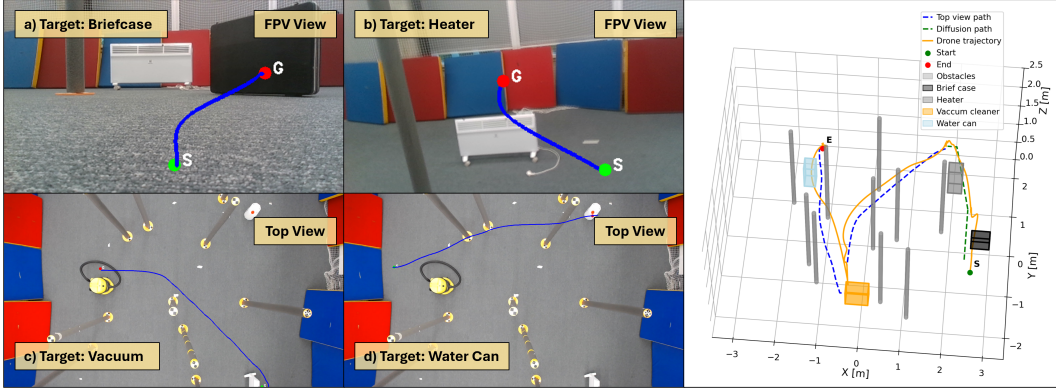


Figure 5: Scenario 3: Long-horizon multi-target navigation using sequential FPV and top-view planning.

4.3 Scenario 3: Long-Horizon Multi-Target Navigation

The third experiment evaluated the proposed framework in a long-horizon multi-target navigation task, as illustrated in Fig. 5. The user prompt was: “find the briefcase, vacuum cleaner, heater, and the water can.” During mission initialization, the agent determined that the briefcase and heater were more suitable for FPV navigation, while the vacuum cleaner and water can were better represented in the top-view observation. The generated mission plan therefore first executed FPV navigation toward the briefcase and heater, followed by top-view navigation toward the vacuum cleaner and water can. This experiment demonstrates the capability of the proposed framework to perform long-horizon semantic navigation using mission-level multi-view reasoning and sequential planner execution. The framework achieved a success rate of 70% (7/10 trials), while the remaining failures were caused by NMPC local deadlock behavior near obstacles.

4.4 Scenario 4: Semantic Reasoning for Safe Landing Site Selection

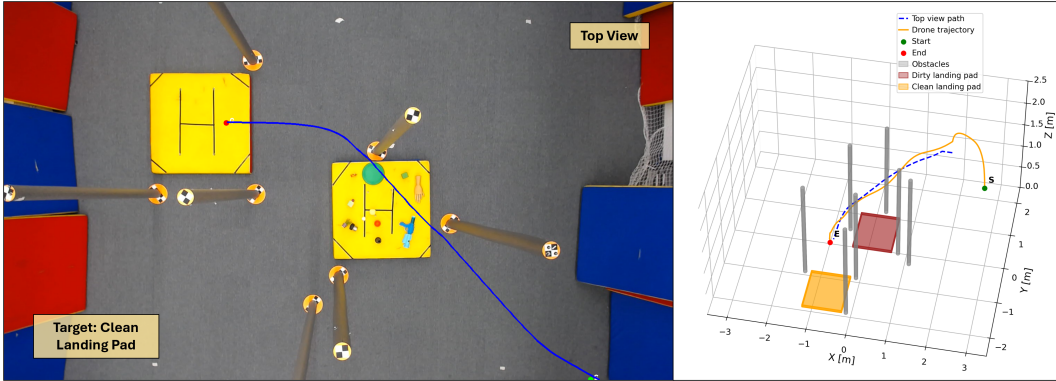


Figure 6: Scenario 4: Multi-view reasoning for safe landing-site selection using obstacle distribution and environmental context analysis.

The fourth experiment evaluated the semantic reasoning capability of the proposed framework for safe landing-site selection, as shown in Fig. 6. The environment contained two candidate landing sites with different surrounding obstacle distributions. The user prompt instructed the agent to “find the cleanest landing site for the drone.” Although both landing sites were partially visible in the FPV view, the top-view observation provided clearer semantic and spatial context for safe landing-site selection. During mission initialization, the agent analyzed the environmental context around both landing sites and selected the less cluttered region as the safer landing target. The generated mission plan then executed top-view trajectory planning toward the selected landing location. This experiment demonstrates the ability of the proposed framework to perform high-level semantic rea-

soning beyond target localization by incorporating environmental context into navigation decisions. The framework achieved a success rate of 100% (10/10 trials).

4.5 Discussion

Across all experiments, the diffusion planners consistently generated feasible navigation trajectories, achieving a trajectory generation success rate of 100%. The overall mission success rate across all scenarios was 80%, while the end-to-end inference time ranged from 20 to 100 seconds depending on the number of targets specified in the user instruction. The experiments further demonstrated the importance of coordinated multi-view reasoning for indoor UAV navigation. In several scenarios, targets that were partially occluded or difficult to distinguish in the FPV observation were more clearly identifiable in the top-view image, while nearby targets benefited from the detailed local visibility provided by FPV navigation. By jointly reasoning across synchronized FPV and top-view observations during mission initialization, the proposed framework improved planner selection, reduced repeated target exploration, and minimized unnecessary replanning during long-horizon navigation tasks. Although prior works explored multi-view perception and navigation, existing approaches do not perform coordinated mission-level reasoning across synchronized FPV and top-view observations for long-horizon UAV navigation. Therefore, direct quantitative comparison with prior methods was not conducted.

4.6 Limitations

Despite the promising performance of the proposed **AgenticDiffusion** framework, several limitations remain. First, the current experimental setup relies on VICON infrastructure for obstacle localization and for tracking semantic targets during mission execution. Although target identification is performed using open-vocabulary grounding and image-to-world projection, mission-state monitoring and target-completion verification depend on VICON-tracked objects. Consequently, the framework remains partially dependent on external motion-capture infrastructure. Second, the experimental validation is constrained by the limited size of the indoor flight arena. The available VICON capture area is approximately $3 \times 3 \text{ m}^2$, while the effective top-view coverage is approximately $2 \times 2 \text{ m}^2$, restricting the scale of the navigation tasks.

5 Conclusion

This paper presented **AgenticDiffusion**, a multi-view UAV navigation framework that combines language-guided reasoning, open-vocabulary target grounding, vision-based diffusion trajectory planning, and NMPC-based control within a unified aerial navigation pipeline. The proposed framework jointly reasons across synchronized FPV and top-view observations to determine the most suitable viewpoint and planner for each navigation task prior to trajectory execution. By leveraging complementary viewpoints during mission initialization, the framework improves target visibility analysis, reduces repeated exploration, and enables efficient long-horizon navigation in cluttered indoor environments. Unlike conventional single-view navigation pipelines, the proposed approach performs coordinated mission-level reasoning before execution, enabling planner-aware navigation across heterogeneous visual observations.

The framework was validated in four real-world indoor UAV navigation scenarios involving adaptive viewpoint selection, sequential target navigation, long-horizon mission execution, and landing-site reasoning. Experimental results demonstrated an overall mission success rate of 80% across 40 real-world trials, while the diffusion planners achieved a trajectory generation success rate of 100%. Future work will focus on reducing reliance on external motion-capture infrastructure through onboard perception and mapping, integrating vision-based obstacle detection and target tracking, improving NMPC robustness under constrained flight regions, and evaluating the framework in larger and more complex indoor environments.

References

- [1] Z. Xu, X. Han, H. Shen, H. Jin, and K. Shimada. NavRL: Learning Safe Flight in Dynamic Environments. *IEEE Robotics and Automation Letters*, 10(4):3668–3675, Feb, 26, 2025.
- [2] W. Cai, J. Peng, Y. Yang, Y. Zhang, M. Wei, H. Wang, Y. Chen, T. Wang, and J. Pang. NavDP: Learning Sim-to-Real Navigation Diffusion Policy with Privileged Information Guidance, 2025. arXiv:2505.08712.
- [3] A. Sridhar, D. Shah, C. Glossop, and S. Levine. NoMaD: Goal Masked Diffusion Policies for Navigation and Exploration. In *Proc. IEEE Int. Conf. on Robotics and Automation (ICRA)*, pages 63–70, May 13-17, 2024.
- [4] J. Zhang, K. Wang, R. Xu, G. Zhou, Y. Hong, X. Fang, et al. NaVid: Video-based VLM Plans the Next Step for Vision-and-Language Navigation. *Robotics: Science and Systems*, 2024.
- [5] S. Liu, Z. Zeng, T. Ren, F. Li, H. Zhang, J. Yang, et al. Grounding DINO: Marrying DINO with Grounded Pre-Training for Open-Set Object Detection. In *Proc. European Conference on Computer Vision*, page 38–55, 2024.
- [6] C. Castellani, E. Turco, and D. Prattichizzo. 3D RL-DWA: A Hybrid Reinforcement Learning and Dynamic Window Approach for Goal-Directed Local Navigation in Multi-DoF Robots, 2026. arxiv:2605.12689.
- [7] S. Hakenes and T. Glasmachers. Deep Reinforcement Learning Based Navigation with Macro Actions and Topological Maps, 2025. arxiv:2504.18300.
- [8] J. Liu, M. Stamatopoulou, and D. Kanoulas. DiPPeR: Diffusion-based 2D Path Planner applied on Legged Robots. In *Proc. IEEE Int. Conf. on Robotics and Automation (ICRA)*, pages 9264–9270, May 13-17, 2024.
- [9] M. Stamatopoulou, J. Liu, and D. Kanoulas. DiPPeST: Diffusion-based Path Planner for Synthesizing Trajectories Applied on Quadrupe Robots. In *Proc. IEEE Int. Conf. on Intelligent Robots and Systems (IROS)*, pages 7787–7793, Oct. 14-18, 2024.
- [10] J. Liang, A. Payandeh, D. Song, X. Xiao, and D. Manocha. DTG: Diffusion-based Trajectory Generation for Mapless Global Navigation. In *Proc. IEEE Int. Conf. on Intelligent Robots and Systems (IROS)*, pages 5340–5347, Oct. 14-18, 2024.
- [11] Y. Zeng, H. Ren, S. Wang, J. Huang, and H. Cheng. NaviDiffusor: Cost-Guided Diffusion Model for Visual Navigation. In *Proc. IEEE Int. Conf. on Robotics and Automation (ICRA)*, pages 11994–12001, May 20-23, 2025.
- [12] X. Liu, V. Armstrong, S. Nabil, and C. Muise. Exploring multi-view perspectives on deep reinforcement learning agents for embodied object navigation in virtual home environments. In *Proc. of Int. Conf. on Computer Science and Software Engineering (CASCON)*, page 190–195, Nov. 22-25, 2021.
- [13] S. Yang, S. A. Scherer, X. Yi, and A. Zell. Multi-camera visual SLAM for autonomous navigation of micro aerial vehicles. *Robotics and Autonomous Systems*, 93:116–134, July 2017.
- [14] K. Zhu, W. Chen, W. Zhang, R. Song, and Y. Li. Autonomous Robot Navigation Based on Multi-Camera Perception. In *Proc. IEEE/RSJ Int. Conf. on Intelligent Robots and Systems (IROS)*, pages 5879–5885, 2020.
- [15] H. Lu, M. Chiquier, and C. Vondrick. Private multiparty perception for navigation. In *Proc. of the Int. Conf. on Neural Information Processing Systems (NeurIPS)*, pages 3318–3328, Nov.-Dec. 28-09, 2022.

- [16] T. Xu, J. Chen, J. Zhang, W. Zhang, Z. Qi, M. Li, Z. Zhang, and H. Wang. MM-Nav: Multi-View VLA Model for Robust Visual Navigation via Multi-Expert Learning, 2025. arxiv:2510.03142.
- [17] C. Huang, O. Mees, A. Zeng, and W. Burgard. Visual Language Maps for Robot Navigation. In *Proc. IEEE Int. Conf. on Robotics and Automation (ICRA)*, pages 10608–10615, May-June, 29-2, 2023.
- [18] B. Chen, Z. Xu, S. Kirmani, B. Ichter, D. Sadigh, L. Guibas, and F. Xia. SpatialVLM: Endowing Vision-Language Models with Spatial Reasoning Capabilities. In *Proc. IEEE/CVF Conf. on Computer Vision and Pattern Recognition (CVPR)*, pages 14455–14465, June 16-22, 2024.
- [19] L. Zhang, X. Hao, Q. Xu, Q. Zhang, X. Zhang, P. Wang, J. Zhang, Z. Wang, S. Zhang, and R. Xu. MapNav: A Novel Memory Representation via Annotated Semantic Maps for Vision-and-Language Navigation, 2026. arxiv:2502.13451.
- [20] S. Lee, D. Ekpo, H. Liu, F. Huang, A. Shrivastava, and J.-B. Huang. Imagine, Verify, Execute: Memory-guided Agentic Exploration with Vision-Language Models. In *Conference on Robot Learning (CoRL)*, pages 4837–4858, Sept. 27-30, 2025.
- [21] Z. Wang and X. Yang. Enhancing Vision-and-Language Navigation in Continuous Environment via Data Synthesis. In *Proc. IEEE Int. Conf. on Neural Networks, Information and Communication Engineering (NNICE)*, pages 713–716, Jan. 10-12, 2025.
- [22] X. Shi, Z. Li, Y. Qiao, and Q. Wu. Fast-SmartWay: Panoramic-Free End-to-End Zero-Shot Vision-and-Language Navigation, 2025. arxiv:2511.00933.
- [23] S. Zeng, D. Qi, X. Chang, F. Xiong, X. Shichao, X. Wu, et al. JanusVLN: Decoupling Semantics and Spatiality with Dual Implicit Memory for Vision-Language Navigation. In *Int. Conf. on Learning Representations*, April 23-25, 2026.
- [24] Z. Xin, W. Li, Y. Jiang, Z. Huang, B. Wang, P. Li, et al. AgentVLN: Towards Agentic Vision-and-Language Navigation, 2026. arxiv:2603.17670.
- [25] X. Wang, D. Yang, Z. Wang, H. Kwan, J. Chen, W. Wu, et al. Towards Realistic UAV Vision-Language Navigation: Platform, Benchmark, and Methodology. In *Int. Conf. on Learning Representations*, April 24-28, 2025.
- [26] G. Wang, Y. Xie, Y. Jiang, A. Mandlekar, C. Xiao, Y. Zhu, L. Fan, and A. Anandkumar. Voyager: An Open-Ended Embodied Agent with Large Language Models. *Transactions on Machine Learning Research*, March 2024.
- [27] S. S. Kannan, V. L. N. Venkatesh, and B.-C. Min. SMART-LLM: Smart Multi-Agent Robot Task Planning using Large Language Models. In *Proc. IEEE/RSJ Int. Conf. on Intelligent Robots and Systems (IROS)*, pages 12140–12147, Oct. 14-18, 2024.
- [28] A Hierarchical Agentic Framework for Autonomous Drone-Based Visual Inspection, author=Ethan Herron and Xian Yeow Lee and Gregory Sin and Teresa Gonzalez Diaz and Ahmed Farahat and Chetan Gupta, 2025. arxiv:2510.00259.
- [29] J. Sam, N. Khang, Y. Mahmoud, M. A. Cabrera, and D. Tsetserukou. Action Agent: Agentic Video Generation Meets Flow-Constrained Diffusion, 2026. arxiv:2605.01477.
- [30] OpenClaw Contributors. Openclaw: Open-source agentic ai framework. <https://github.com/openclaw/openclaw>, 2026. GitHub repository, Accessed: 2026-05-27.
- [31] Anthropic. Claude sonnet. <https://www.anthropic.com/claude/sonnet>, 2026. Accessed: 2026-05-27.

- [32] J. A. E. Andersson, J. Gillis, G. Horn, J. B. Rawlings, and M. Diehl. CasADi – A software framework for nonlinear optimization and optimal control. *Mathematical Programming Computation*, 11(1):1–36, 2019.
- [33] R. Verschueren, G. Frison, D. Kouzoupis, J. Frey, N. van Duijkeren, A. Zanelli, B. Novoselnik, T. Albin, R. Quirynen, and M. Diehl. acados – a modular open-source framework for fast embedded optimal control. *Mathematical Programming Computation*, 2021.
- [34] ProcTHOR: Procedural Generation for Embodied AI. <https://procthor.allenai.org/>, 2026. Accessed: 2026-02-20.

Appendix

A Diffusion-Based Trajectory Planning

The proposed top-view diffusion planner is formulated as a conditional UNet-based diffusion model for long-horizon trajectory generation in cluttered indoor environments. The planner predicts a pixel-space trajectory mask conditioned on the start point, goal point, and top-view scene observation. Unlike conventional diffusion frameworks that predict the injected noise directly, the proposed model predicts the denoised trajectory mask at each diffusion step, which is subsequently used in the DDPM posterior during reverse diffusion.

The input representation is formulated as a three-channel tensor:

$$x_0 \in \mathbb{R}^{B \times 3 \times H \times W}, \quad (1)$$

where B denotes the batch size and H and W represent the spatial image dimensions. The three channels correspond to the start-point mask, goal-point mask, and trajectory mask, respectively.

B Forward Diffusion Process.

During training, Gaussian noise is progressively added to the clean trajectory mask using a squared-cosine variance schedule. The forward diffusion process is defined as:

$$x_t = \sqrt{\bar{\alpha}_t} x_0 + \sqrt{1 - \bar{\alpha}_t} \epsilon, \quad (2)$$

where x_t denotes the noisy trajectory sample at diffusion timestep t , $\epsilon \sim \mathcal{N}(0, I)$ represents Gaussian noise, and:

$$\alpha_t = 1 - \beta_t, \quad (3)$$

with β_t denoting the variance schedule. The cumulative diffusion coefficient is:

$$\bar{\alpha}_t = \prod_{s=1}^t \alpha_s. \quad (4)$$

The forward process gradually corrupts the trajectory representation while preserving the start and goal conditioning information.

C Reverse Denoising Process.

During inference, the conditional UNet iteratively predicts the denoised trajectory mask \hat{x}_0 from the noisy sample x_t . The predicted clean trajectory mask is then used in the DDPM posterior to compute the next denoised sample:

$$x_{t-1} = \mu_t(x_t, \hat{x}_0) + \sigma_t z, \quad z \sim \mathcal{N}(0, I), \quad (5)$$

where μ_t and σ_t denote the posterior mean and variance, respectively. The reverse denoising process iterates from $t = T$ to $t = 0$, where T is the total number of diffusion timesteps.

To preserve boundary consistency during trajectory generation, the start and goal channels are inpainted at each denoising iteration. This ensures that the generated trajectory remains aligned with the specified navigation endpoints throughout the diffusion process.

D Training Objective.

The diffusion planner is trained using a weighted objective consisting of trajectory reconstruction and endpoint reconstruction losses:

$$\mathcal{L} = \lambda_{\text{path}} L_{\text{path}} + \lambda_{\text{endpoint}} L_{\text{endpoint}}, \quad (6)$$

where λ_{path} and $\lambda_{\text{endpoint}}$ control the contributions of trajectory reconstruction and endpoint accuracy, respectively.

The trajectory reconstruction loss is formulated as:

$$L_{\text{path}} = w_t \frac{1}{N} \sum_{B,H,W} \left(T_{B,H,W}^{\text{pred}} - T_{B,H,W}^{\text{gt}} \right)^2, \quad (7)$$

where T^{pred} and T^{gt} denote the predicted and ground-truth trajectory masks, respectively, w_t is the trajectory-channel weight, and:

$$N = B \times H \times W \quad (8)$$

is the total number of pixels across the batch.

To enforce accurate boundary conditions, the endpoint reconstruction loss is additionally introduced:

$$L_{\text{endpoint}} = \frac{1}{2} [w_s \mathcal{L}_s + w_g \mathcal{L}_g], \quad (9)$$

where w_s and w_g denote the weights associated with the start-point and goal-point reconstruction losses, respectively.

The start-point reconstruction loss is defined as:

$$\mathcal{L}_s = \frac{1}{N} \sum_{B,H,W} \left(S_{B,H,W}^{\text{pred}} - S_{B,H,W}^{\text{gt}} \right)^2, \quad (10)$$

where S^{pred} and S^{gt} denote the predicted and ground-truth start-point masks.

Similarly, the goal-point reconstruction loss is:

$$\mathcal{L}_g = \frac{1}{N} \sum_{B,H,W} \left(G_{B,H,W}^{\text{pred}} - G_{B,H,W}^{\text{gt}} \right)^2, \quad (11)$$

where G^{pred} and G^{gt} represent the predicted and ground-truth goal-point masks, respectively.

The trajectory reconstruction loss enforces global geometric consistency of the generated path, while the endpoint reconstruction losses ensure that the predicted trajectory remains accurately constrained between the desired start and goal locations.

E Training Dataset and Pipeline.

The top-view diffusion planner was trained entirely in simulation using trajectories generated with the A* planner in the ProcTHOR indoor environment dataset [34]. A total of 10,000 trajectories were generated for training, along with 1,500 validation samples and 1,647 testing samples.

All generated trajectories were constrained to traversable regions of the environment, thereby implicitly enforcing collision-free navigation behavior during training. The dataset contains diverse indoor layouts, obstacle configurations, and start-goal pairs to improve generalization across unseen environments.

Training was performed using 100 diffusion timesteps for 30 epochs, which provided the best empirical performance. Although separate diffusion planners were trained for top-view and FPV navigation, both planners followed the same diffusion architecture and training methodology, differing primarily in the visual modality and dataset used for trajectory generation.

F NMPC Formulation

The prediction model used inside the NMPC is represented by a continuous-time quadrotor model which is governed by 13 states where $p_W = [p_x, p_y, p_z]^T$ are the position coordinates in the world frame, $v_W = [v_x, v_y, v_z]^T$ are the linear velocity components in the world frame, $q_B = (q_w, q_x, q_y, q_z)^T$ are the quaternions for the orientation of the drone's body, and finally $\omega_B = [\omega_x, \omega_y, \omega_z]^T$ are the body angular rates. These states are used to define the first-order nonlinear ordinary differential equations of the quadrotor as shown in Eq. (12).

$$\dot{\mathbf{x}} = \begin{bmatrix} \dot{p}_W \\ \dot{v}_W \\ \dot{q}_B \\ \dot{\omega}_B \end{bmatrix} = \begin{bmatrix} v_W \\ R(q) \frac{T_B}{m} + g \\ \frac{1}{2} q_{\omega B} \cdot q_B \\ J^{-1} (\tau_B - \omega_B \times J \omega_B) \end{bmatrix}, \quad (12)$$

where $R(q)$ is the quaternion rotational matrix, $T_B = [0, 0, \sum_{i=1}^4 T_i]^T$ is the total thrust, g is the gravitational vector $g = [0, 0, 9.81]^T$, $J = \text{diag}(J_x, J_y, J_z)$ is the diagonal of the inertia matrix, $q_{\omega} = (0, \omega_x, \omega_y, \omega_z)^T$ is the angular velocity quaternion and τ_B is the body torque matrix as shown in Eq. (13)

$$\tau_B = \begin{bmatrix} -l_y & l_y & l_y & -l_y \\ -l_x & -l_x & l_x & l_x \\ k_t & -k_t & k_t & -k_t \end{bmatrix} \begin{bmatrix} \mathbf{u}_1 \\ \mathbf{u}_2 \\ \mathbf{u}_3 \\ \mathbf{u}_4 \end{bmatrix}, \quad (13)$$

where $\mathbf{u}_1, \mathbf{u}_2, \mathbf{u}_3, \mathbf{u}_4$ are the input motor forces, l_x, l_y are the distances to the x -axis and y -axis, respectively and, k_t is the torque constant. This matrix according to the free body diagram shown in Fig. 7

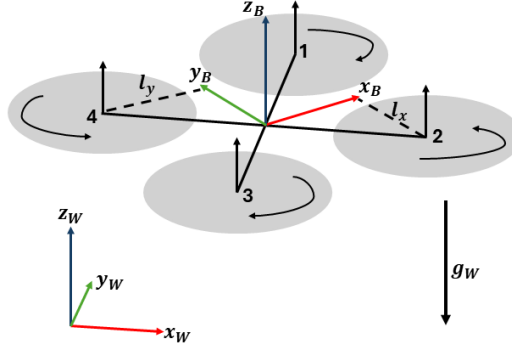


Figure 7: Drone free-body diagram.

The reference trajectory is constructed from the planned path using a spatial progress variable s . Let the path be represented as

$$\mathcal{P} = \left\{ \mathbf{p}_j^{\text{path}} \right\}_{j=1}^M, \quad \mathbf{p}_j^{\text{path}} = [x_j \quad y_j \quad z_j]^T. \quad (14)$$

The path is parameterized by its arc length $s \in [0, L]$, giving the interpolated reference position

$$\mathbf{p}^{\text{ref}}(s) = \begin{bmatrix} x^{\text{ref}}(s) \\ y^{\text{ref}}(s) \\ z^{\text{ref}}(s) \end{bmatrix}. \quad (15)$$

At time step k , the reference progress along the horizon is given by

$$s_{k+i} = \min(s_k + i\Delta s, L), \quad i = 0, \dots, N, \quad (16)$$

where Δs is the spatial reference step. The desired yaw angle is aligned with the local path tangent,

$$\psi^{\text{ref}}(s) = \text{atan2} \left(\frac{dy^{\text{ref}}}{ds}, \frac{dx^{\text{ref}}}{ds} \right). \quad (17)$$

The corresponding quaternion reference becomes:

$$\mathbf{q}^{\text{ref}}(s_{k+i}) = \text{quat}(0, 0, \psi^{\text{ref}}(s_{k+i})). \quad (18)$$

The input reference is chosen as the hover thrust equally distributed across the four motors,

$$\mathbf{u}_{k+i}^{\text{ref}} = \frac{mg}{4} [1 \ 1 \ 1 \ 1]^\top. \quad (19)$$

To formulate the nonlinear least-squares objective, we define the NMPC output residual as Eq. (20)

$$\mathbf{r}_i = \mathbf{y}_i - \mathbf{y}_i^{\text{ref}}, \mathbf{r}_N = \mathbf{y}_N - \mathbf{y}_N^{\text{ref}}, \quad (20)$$

where the stage output and the corresponding reference are:

$$\mathbf{y}_i = \begin{bmatrix} \mathbf{p}_i \\ \mathbf{v}_i \\ \mathbf{e}_{q,i} \\ \boldsymbol{\omega}_i \\ \mathbf{u}_i \\ \mathbf{h}_{\text{obs}}(\mathbf{x}_i) \end{bmatrix}, \mathbf{y}_i^{\text{ref}} = \begin{bmatrix} \mathbf{p}_i^{\text{ref}} \\ \mathbf{v}_i^{\text{ref}} \\ \mathbf{0}_3 \\ \boldsymbol{\omega}_i^{\text{ref}} \\ \mathbf{u}_i^{\text{ref}} \\ \mathbf{0}_{n_o} \end{bmatrix}, \mathbf{y}_N = \begin{bmatrix} \mathbf{p}_N \\ \mathbf{v}_N \\ \mathbf{e}_{q,N} \\ \boldsymbol{\omega}_N \\ \mathbf{h}_{\text{obs}}(\mathbf{x}_N) \end{bmatrix}, \mathbf{y}_N^{\text{ref}} = \begin{bmatrix} \mathbf{p}_N^{\text{ref}} \\ \mathbf{v}_N^{\text{ref}} \\ \mathbf{0}_3 \\ \boldsymbol{\omega}_N^{\text{ref}} \\ \mathbf{0}_{n_o} \end{bmatrix} \quad (21)$$

The attitude tracking error is computed using the relative quaternion between the current attitude and the reference attitude. Let $\mathbf{q}(k)$ be the current quaternion and $\mathbf{q}_r(k)$ be the reference quaternion. The relative quaternion is

$$\mathbf{q}_e(k) = \mathbf{q}_r^{-1}(k) \otimes \mathbf{q}(k), \quad (22)$$

where \otimes denotes quaternion multiplication. Since quaternions have a double-cover representation, the error quaternion is mapped to a consistent hemisphere as

$$\tilde{\mathbf{q}}_e(k) = \begin{cases} \mathbf{q}_e(k), & q_{e,0}(k) \geq 0, \\ -\mathbf{q}_e(k), & q_{e,0}(k) < 0. \end{cases} \quad (23)$$

The attitude residual used in the NMPC cost is the vector part of this quaternion error:

$$\mathbf{e}_q(k) = \text{vec}(\tilde{\mathbf{q}}_e(k)) = [\tilde{q}_{e,1}(k) \ \tilde{q}_{e,2}(k) \ \tilde{q}_{e,3}(k)]^T. \quad (24)$$

Obstacle avoidance is incorporated into the NMPC objective using smooth residuals \mathbf{h}_{obs} . Each obstacle is modeled as a vertical cylinder:

$$\mathcal{O}_j = (c_{x,j}, c_{y,j}, r_j, h_j), \quad j = 1, \dots, n_o, \quad (25)$$

where $(c_{x,j}, c_{y,j})$ is the obstacle center in the horizontal plane, r_j is the physical obstacle radius, and h_j is the obstacle height. For the quadrotor position $[x_i, y_i, z_i]$, the horizontal distance to obstacle j is:

$$d_{j,i} = \sqrt{(x_i - c_{x,j})^2 + (y_i - c_{y,j})^2} + \epsilon, \quad (26)$$

where $\epsilon > 0$ is a small constant used for numerical regularization. The horizontal penetration residual is computed using a smooth softplus function,

$$\eta_{j,i} = \frac{1}{\alpha} \log(1 + \exp(\alpha(r_j^{\text{safe}} - d_{j,i}))), \quad (27)$$

where r_j^{safe} is the safe horizontal radius and $\alpha > 0$ controls the sharpness of the softplus approximation. Since the obstacle is a finite-height cylinder, the horizontal penalty is activated only within the vertical obstacle region. This is achieved using a smooth vertical activation function:

$$\gamma_{j,i}^z = \frac{1}{2} (1 + \tanh(\kappa z_i)) \cdot \frac{1}{2} (1 - \tanh(\kappa [z_i - (h_j + m_z)])), \quad (28)$$

where $\kappa > 0$ controls the sharpness of the vertical activation and m_z is the vertical safety margin. The final obstacle residual for obstacle j is:

$$h_{\text{obs},j}(\mathbf{x}_i) = \gamma_{j,i}^z \eta_{j,i}. \quad (29)$$

Stacking all obstacle residuals gives:

$$\mathbf{h}_{\text{obs}}(\mathbf{x}_i) = \begin{bmatrix} h_{\text{obs},1}(\mathbf{x}_i) \\ h_{\text{obs},2}(\mathbf{x}_i) \\ \vdots \\ h_{\text{obs},n_o}(\mathbf{x}_i) \end{bmatrix}. \quad (30)$$

This formulation keeps the obstacle avoidance term differentiable, making it suitable for gradient-based NMPC solvers. The penalty is approximately zero outside the obstacle safety region and increases smoothly when the quadrotor approaches or enters the safety radius.

Finally, at each time step, the following optimization problem is solved:

$$\begin{aligned} \min_{\mathbf{x}_{0:N}, \mathbf{u}_{0:N-1}} \quad & \sum_{i=0}^{N-1} \frac{1}{2} \|\mathbf{y}_i - \mathbf{y}_i^{\text{ref}}\|_W^2 + \frac{1}{2} \|\mathbf{y}_N - \mathbf{y}_N^{\text{ref}}\|_{W_N}^2 \\ \text{s.t.} \quad & \mathbf{x}_{i+1} = f_{RK4}(\mathbf{x}_i, \mathbf{u}_i), \quad \forall i \in [0, N-1] \\ & \mathbf{u}_{\min} \leq \mathbf{u}_i \leq \mathbf{u}_{\max}, \quad \forall i \in [0, N-1] \\ & \mathbf{x}_{\min} \leq \mathbf{x}_i \leq \mathbf{x}_{\max}, \quad \forall i \in [0, N] \end{aligned} \quad (31)$$

where the stage and terminal weights are:

$$W = \text{blkdiag}(Q_p, Q_v, Q_q, Q_\omega, R, w_{\text{obs}} I_{n_o}), \quad (32)$$

$$W_N = \text{blkdiag}(Q_p, Q_v, Q_q, Q_\omega, w_{\text{obs}} I_{n_o}), \quad (33)$$